Chemistry
A European
Journal

Chemistry Europe
European Chemical Societies Publishing

Accepted Article

Title: Balanced Energy Gaps as a Key Design Rule for Solution-Phase Organic Room Temperature Phosphorescence

Authors: Simon Paredis, Tom Cardeynaels, Suman Kuila, Jasper Deckers, Melissa Van Landeghem, Koen Vandewal, Andrew Danos, Andrew P. Monkman, Benoît Champagne, and Wouter Maes

To be cited as: *Chem. Eur. J.* **2023**, e202301369

Link to VoR: https://doi.org/10.1002/chem.202301369

WILEY VCH

10.1002/chem.202301369

WILEY-VCH

RESEARCH ARTICLE

Balanced Energy Gaps as a Key Design Rule for Solution-Phase Organic Room Temperature Phosphorescence

Simon Paredis,[a,b,c] Tom Cardeynaels,[a,b,c,d] Suman Kuila,[e] Jasper Deckers,[a,b,c] Melissa Van Landeghem,[b,c] Koen Vandewal,[b,c] Andrew Danos,*[e] Andrew P. Monkman,[e] Benoît Champagne[d] and Wouter Maes*[a,b,c]

[a] S. Paredis, Dr. T. Cardeynaels, Dr. J. Deckers, Prof. W. Maes
Design & Synthesis of Organic Semiconductors (DSOS), Institute for Materials Research (IMO-IMOMEC)
Hasselt University
Agoralaan 1, 3590 Diepenbeek, Belgium
E-mail: wouter.maes@uhasselt.be

[b] S. Paredis, Dr. T. Cardeynaels, Dr. J. Deckers, Dr. M. Van Landeghem, Prof. K. Vandewal, Prof. W. Maes
IMOMEC Division
IMEC
Wetenschapspark 1, 3590 Diepenbeek, Belgium

[c] S. Paredis, Dr. T. Cardeynaels, Dr. J. Deckers, Dr. M. Van Landeghem, Prof. K. Vandewal, Prof. W. Maes
Energyville
Thorpark, 3600 Genk, Belgium

[d] Dr. T. Cardeynaels, Prof. B. Champagne
Laboratory of Theoretical Chemistry, Theoretical and Structural Physical Chemistry Unit, Namur Institute of Structured Matter
University of Namur
Rue de Bruxelles 61, 5000 Namur, Belgium

[e] Dr. S. Kuila, Dr. A. Danos, Prof. A. P. Monkman
OEM group, Department of Physics
Durham University
South Road, Durham DH1 3LE, United Kingdom
E-mail: andrew.danos@durham.ac.uk

Supporting information for this article is given via a link at the end of the document.

Abstract: Metal-free organic emitters that display solution-phase room temperature phosphorescence (sRTP) remain exceedingly rare. Here, we investigate the structural and photophysical properties that support sRTP by comparing a recently reported sRTP compound (BTaz-Th-PXZ) to two novel analogous materials, replacing the donor group by either acridine or phenothiazine. The emissive triplet excited state remains fixed in all three cases, while the emissive charge-transfer singlet states (and the calculated paired charge-transfer T_2 state) vary with the donor unit. While all three materials show dominant RTP in film, in solution different singlet-triplet and triplet-triplet energy gaps give rise to triplet-triplet annihilation followed by weak sRTP for the new compounds, compared to dominant sRTP throughout for the original PXZ material. Engineering both the sRTP state and higher charge-transfer states therefore emerges as a crucial element in designing emitters capable of sRTP.

Introduction

Organic molecules showing room temperature phosphorescence (RTP) are gaining increasing attention due to their long-lived triplet excited states and emission with large apparent Stokes shifts,[1] rendering these materials attractive for biomedical applications such as bioimaging and antibacterial therapies. Moreover, from a fundamental point of view, phosphorescence is a highly interesting phenomenon because of its spin-forbidden nature. Until recently, the development of organic phosphorescent materials was generally achieved by introducing heavy metals to realize large spin-orbit coupling (SOC) values and thereby allow mixing between excited singlet and triplet states, facilitating intersystem crossing (ISC) and emission from triplet states.[2] However, this approach has drawbacks due to the toxic nature, scarcity, and/or cost of some of the required heavy metals (*e.g.* iridium and platinum).[3] In recent years, more efforts have therefore been devoted to the development of metal-free 'all-organic' phosphorescent molecules.[4]

The design of purely organic RTP emitters is challenging because of their significantly lower SOC values, which limits both the efficiency of the ISC process and emission from the triplet state. Scientists have developed design strategies to enhance SOC in all-organic molecules, such as introducing carbonyl groups, halogen atoms, heteroatoms, or creating high molecular distortion. However, additional efforts are required to optimize the RTP properties.[5] After enabling triplet formation *via* ISC, up-conversion mechanisms such as triplet-triplet annihilation (TTA)[6,7] or thermally activated delayed fluorescence (TADF)[8], which are usually faster than the spin-forbidden phosphorescence process, must be suppressed to achieve highly efficient phosphorescent organic molecules. This can be done by decreasing the emitter concentration (limiting bimolecular TTA) or by more sophisticated molecular design.[9] Even more critical for the appearance of phosphorescence is the suppression of fast non-radiative relaxation from the excited triplet state to the ground state, caused by for example collisions with solvent molecules and/or oxygen triplet quenching.[10] This can be realized by controlling the molecular packing, *i.e.* doping the emitter in a rigid host material,[11] crystallization,[12] or the introduction of organic frameworks.[13] Without the benefits of a rigid environment, it becomes especially

10.1002/chem.202301369

challenging to develop materials that exhibit RTP in solution (sRTP), as the increased molecular motions and vibrational degrees of freedom greatly enhance non-radiative decay in competition with triplet emission.[14] Therefore, the most efficient sRTP systems to date utilize non-covalent interactions in a host-guest supramolecular microenvironment to alleviate these non-radiative decay pathways for enhanced triplet stability.[15,16] However, the majority of sRTP systems studied so far utilize either heavy halogen atoms (Br or I) in the molecular framework or in a combination with carbonyl groups to enhance the intersystem crossing, following the El-Sayed rule.[15-17]

New design principles that allow manipulation of excited state dynamics to obtain sRTP promise transforming applications in sensing and biological imaging technologies.[18] The rarity of matrix-free purely organic sRTP and limited molecular design principles to achieve efficient sRTP imply that the design rules to enable this property remain largely unknown.

Recently, we reported a series of donor-π-bridge-acceptor (D-π-A) all-organic emitters consisting of a phenoxazine (PXZ) donor moiety and a benzothiazole (BTaz) acceptor moiety, linked together by either a phenyl (Ph), naphthalene (Na), or thiophene (Th) bridging unit.[14] It was shown that the π-bridge has minimal effect on the singlet excited state, but drastically changes the triplet excited state energies. Consequently, the complex interplay between singlet and triplet excited states resulted in TADF for **BTaz-Ph-PXZ** and **BTaz-Na-PXZ**, whereas **BTaz-Th-PXZ** exhibited ISC followed by sRTP. In order to investigate the origin of this fast sRTP, **BTaz-Th-PXZ** is used here as a reference material and compared to new emitters with the donor unit replaced by either 9,9-dimethyl-9,10-dihydroacridine (**BTaz-Th-DMAC**) or phenothiazine (**BTaz-Th-PTZ**). Overall, we find that the choice of donor group controls the energies of the singlet states with charge-transfer (CT) character, but can also lead to dominance of a competing TTA pathway in solution. Guided by density functional theory (DFT) calculations, we propose that the enhanced sRTP in **BTaz-Th-PXZ** occurs by bringing the CT singlet and/or triplet states sufficiently close in energy to allow coupling with the phosphorescent locally excited (LE) triplet state. This coupling results in donating singlet character and/or high SOC (from S_1 or T_2) to the sRTP $T_1 \rightarrow S_0$ transition.[19] In the other materials where these energy gaps are larger and phosphorescence is slower, sRTP is dominated by TTA emission. If these gaps are made too small, TADF emission instead dominates. These results therefore unlock new strategic insight toward designing efficient organic sRTP emitters, and highlight the surprisingly critical role of balancing energy gaps to higher excited states that have previously been overlooked in this class of phosphorescent materials.

Results and Discussion

The acceptor part of the dyads (BTaz-Th-Br) was synthesized according to a literature procedure using sodium metabisulfite in *N*,*N*-dimethylformamide (DMF).[14,20] Afterwards, the brominated acceptor unit was coupled to the three different donors using Buchwald-Hartwig cross-coupling.[14] The catalytic system used consists of palladium(II) acetate ($Pd(OAc)_2$) and tri-*tert*-butylphosphine (P(*t*-Bu)$_3$) in the presence of sodium *tert*-butoxide (Na*t*BuO) in toluene, affording **BTaz-Th-DMAC**, **BTaz-Th-PXZ**, and **BTaz-Th-PTZ** (Scheme 1).

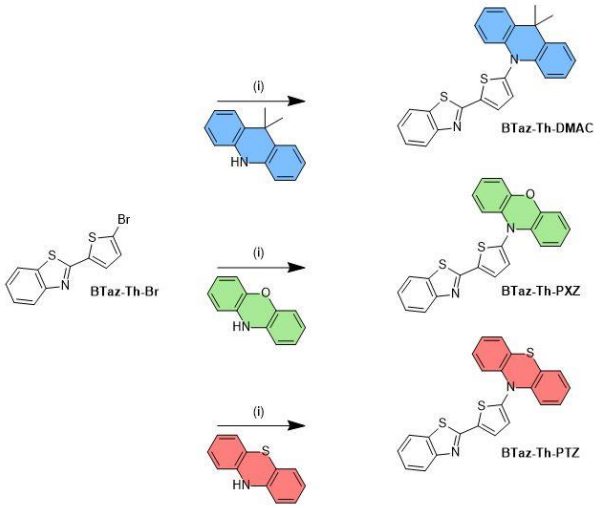

Scheme 1: Synthesis procedure for the BTaz-Th-Donor emitters: (i) $Pd(OAc)_2$, P(*t*-Bu)$_3$, Na*t*BuO, toluene, reflux, 16 h.

In order to calculate the electronic structure and energies, the geometries of **BTaz-Th-DMAC**, **BTaz-Th-PXZ**, and **BTaz-Th-PTZ** were optimized using DFT calculations (M06/6-311G(d)). The singlet and triplet energies were determined using additional time-dependent DFT (TDDFT) calculations using LC-BLYP (ω = 0.17 bohr^{-1}) as the exchange-correlation (XC) functional.[21] The TDDFT calculations were performed under the Tamm-Dancoff approximation (TDA) and the polarizable continuum model (PCM) in cyclohexane to simulate a non-polar environment.

All calculations were performed using the Gaussian16 package.[22] During these TDDFT calculations, the orbital spatial distributions were obtained from single-point calculations, using the same LC-BLYP/6-311G(d) method. The CT character of the involved states was investigated by looking at the differences between ground and excited state electron densities. These CT characters were quantified by the distance over which the electronic charge is transferred (d_{CT}) and the related change in dipole moment ($\Delta\mu$), calculated as described by Le Bahers and coworkers.[23] Furthermore, the SOC values are calculated using the PySOC program using the same XC functional, basis set, and PCM treatment as described before.[24]

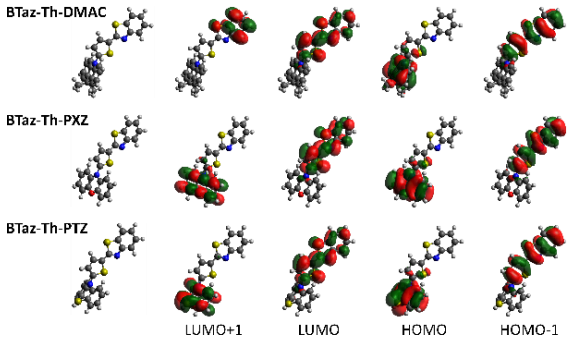

Figure 1: HOMO-LUMO spatial distributions for **BTaz-Th-DMAC**, **BTaz-Th-PXZ**, and **BTaz-Th-PTZ**. Isocontour values of 0.02 (a.u.) were used for all orbitals.

Table 1: TDDFT results for the vertical first and second singlet excitation energies and the corresponding oscillator strengths (*f*), and the first and second vertical triplet excitation energies, as determined with TDDFT-TDA.

Compound	S_1 (eV)	f_{S_1}	S_2 (eV)	f_{S_2}	T_1 (eV)	T_2 (eV)	$\Delta E_{S_1-T_1}$ (eV)	$\Delta E_{S_1-T_2}$ (eV)	$\Delta E_{T_2-T_1}$ (eV)
BTaz-Th-DMAC	3.12	<0.001	3.88	1.080	2.77	3.11	0.35	0.01	0.34
BTaz-Th-PXZ	2.86	<0.001	3.78	0.013	2.78	2.85	0.08	0.01	0.07
BTaz-Th-PTZ	3.19	<0.001	3.78	0.001	2.76	3.14	0.43	0.05	0.38

Table 2: Nature of the various transitions (H = HOMO, L = LUMO), charge-transfer distance (d_{CT}), and change in dipole moment ($\Delta\mu$, excited state dipole – ground state dipole) accompanying the $S_0 \rightarrow S_x$ and $S_0 \rightarrow T_x$ transitions in cyclohexane, as determined with TDDFT-TDA.

Compound	S_1			S_2			T_1			T_2		
	Nature	d_{CT} (Å)	$\Delta\mu$ (D)	Nature	d_{CT} (Å)	$\Delta\mu$ (D)	Nature	d_{CT} (Å)	$\Delta\mu$ (D)	Nature	d_{CT} (Å)	$\Delta\mu$ (D)
BTaz-Th-DMAC	H→L (89%)	3.49	19.30	H-1→L (90%)	0.66	0.66	H-1→L (92%)	0.23	0.44	H→L (89%)	3.48	19.20
BTaz-Th-PXZ	H→L (88%)	3.50	19.03	H→L+1 (96%)	0.54	0.54	H-1→L (92%)	0.35	0.67	H→L (88%)	3.49	18.88
BTaz-Th-PTZ	H→L (84%)	3.63	19.30	H→L+1 (93%)	0.26	0.26	H-1→L (91%)	0.31	0.59	H→L (70%)	3.42	15.05

DFT geometry optimizations illustrate that the BTaz-Th moiety is coplanar, confirming that both parts combined electronically act as the acceptor, as shown in Figure 1.[14] Furthermore, all three donor parts are perpendicular, *i.e.* 90° with respect to the acceptor unit, leading to strong electronic decoupling of donor and acceptor. Moreover, in contrast to the planar DMAC and PXZ, the PTZ unit adopts a butterfly shape, bending along the S-N axis (99°). As a result of the perpendicular and electronically decoupled D-A orientations, the highest occupied molecular orbital (HOMO) and lowest unoccupied molecular orbital (LUMO) are localized on the donor and acceptor parts, respectively, resulting in well-separated HOMO-LUMO topologies. Consequently, strong CT character is observed for the lowest energy excited singlet state of all three dyads. The first excited triplet state shows LE character, while strong CT character is also observed for the second excited triplet state, as illustrated in Figure S1.

The calculated vertical excitation energies for the most relevant excited states are listed in Table 1. A clear decrease in energy of the first excited singlet state is observed for **BTaz-Th-PXZ** with respect to **BTaz-Th-DMAC** and **BTaz-Th-PTZ**, whereas the first triplet state energy remains approximately the same for all three compounds. Moreover, a drop of the second triplet state energy is observed for **BTaz-Th-PXZ**, resulting in a significantly smaller energy splitting between the first two excited triplet states ($\Delta E_{T_2\text{-}T_1}$). Furthermore, there is little difference in CT distance or change in dipole moment for the three dyads, as illustrated in Table 2. Important to note here is that these calculations are based on transitions from and to isolated energy states. Therefore, no interactions between excited states are taken into account. SOC values are shown in Table 3, confirming the effect of the extra 'heavy' sulfur atom in **BTaz-Th-PTZ** (18.21 cm^{-1} compared to 12.27 and 11.63 cm^{-1} for **BTaz-Th-DMAC** and **BTaz-Th-PXZ**, respectively, for $T_2 \rightarrow S_0$). The SOC values for the $T_2 \rightarrow S_0$ transitions are large for all three materials, with much smaller values for other combinations.

Steady-state absorption and fluorescence spectra in toluene and methylcyclohexane (MCH) solution are shown in Figure 2. The absorption spectra consist of one major and one minor, lower energy peak for all three molecules. These two peaks can be attributed to LE singlet and direct CT absorption bands, respectively. These assignments are supported by simulated TDDFT absorption spectra, shown in Figure S2. The relative intensity and the wavelength of the lower energy CT absorption differ for all three emitters. The CT absorption bands of **BTaz-Th-DMAC** and **BTaz-Th-PTZ** are more intense than for **BTaz-Th-PXZ**, with **BTaz-Th-PTZ** being the most intense. Emission spectra were recorded in the same two solvents. The higher energy emission peaks for both dual-emissive **BTaz-Th-PXZ** and **BTaz-Th-PTZ** in toluene can be assigned to LE emission, likely from the donor,[25] whereas **BTaz-Th-DMAC** shows a dominant CT emission band. The possibility of dual stable conformations of the PXZ and PTZ donor units, which could then cause dual emission profiles,[26] was also considered but disregarded due to the large energy difference between perpendicular and coplanar conformations, as shown in the relaxed potential energy surface scans using the M06/6-311G(d) method (Figure S3). In non-polar MCH, the CT states are less red-shifted compared to toluene, causing a more significant overlap with the LE emission. This overlap makes conclusive assignment more difficult, although highlighting the presence of an LE-attributed blue-edge shoulder for **BTaz-Th-DMAC**. Comparing emission in the two solvents, the largest solvatochromic red-shift is observed for the CT band of **BTaz-Th-PTZ** (appearing as a shoulder of the main LE peak, marked on the spectra, and compared directly in Figure S4), indicating a stronger CT character.

Emission quantum yields of the three emitters, both in dilute toluene solution and in 1 w/w% zeonex films and under normal and inert atmosphere ($\Phi_{f,atm}$ and $\Phi_{f,inert}$) were determined and are shown in Table 4. In toluene, a strong decrease of the quantum

Table 3: Spin-orbit coupling values (in cm^{-1}) between the ground and various excited states as obtained using TDDFT calculations with LC-BLYP (ω = 0.17 $bohr^{-1}$)/6-311G(d) under the TDA and applying the PCM (cyclohexane).

Compound	$S_1 \rightarrow T_1$	$S_1 \rightarrow T_2$	$T_1 \rightarrow S_0$	$T_2 \rightarrow S_0$
BTaz-Th-DMAC	1.82	0.01	0.18	12.27
BTaz-Th-PXZ	1.75	0.03	0.13	11.63
BTaz-Th-PTZ	1.17	0.26	0.14	18.21

10.1002/chem.202301369

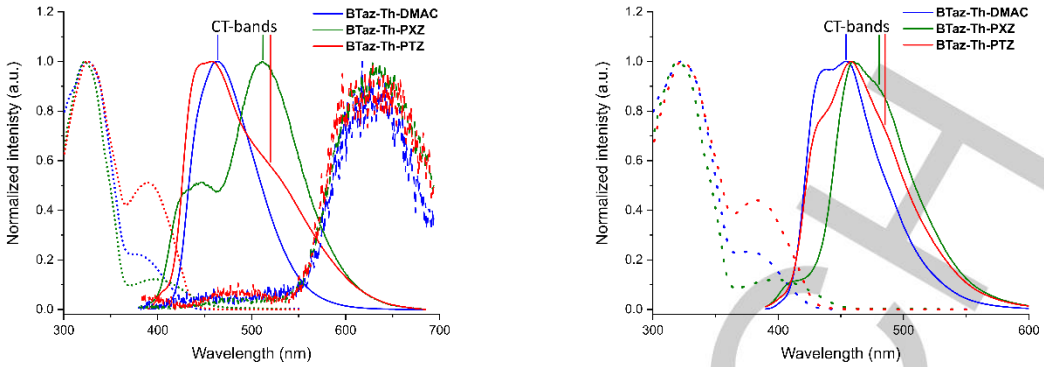

Figure 2: Normalized steady-state absorption spectra (dotted lines), steady-state emission spectra (solid lines), and room temperature phosphorescence spectra (dashed lines; degassed solution, >4 ms delay time) for **BTaz-Th-DMAC** (blue), **BTaz-Th-PXZ** (green), and **BTaz-Th-PTZ** (red) in toluene (left) and in MCH (right).

yield is observed when changing the DMAC donor to PXZ and PTZ. Furthermore, a substantial increase in singlet oxygen quantum yield (Φ_Δ) is observed for **BTaz-Th-PTZ** as compared to **BTaz-Th-DMAC** and **BTaz-Th-PXZ** (Figure S5), which could be explained by the additional 'heavy' sulfur atom in the PTZ donor unit increasing SOC (Table 3) and therefore facilitating ISC, resulting in excellent triplet generation. In zeonex films, **BTaz-Th-DMAC** again possesses the highest quantum yield, followed by **BTaz-Th-PTZ** and **BTaz-Th-PXZ**. In all cases, the difference between the quantum yield in air and inert atmosphere is small, indicating only a small contribution from possible delayed emission or phosphorescence pathways.

Time-resolved emission spectroscopy (TRES) experiments in toluene solution were performed to understand the emission mechanism(s). The contour maps of the normalized TRES experiments at room temperature are shown in Figure 3. For **BTaz-Th-DMAC** in toluene, fast decay of the prompt fluorescence (PF) from a spectrally broad mixture of CT and LE states (reflective of the steady-state emission) is observed until ~20 ns, after which the emission falls below the hardware detection limit. Afterwards, microsecond-range delayed fluorescence (DF) is observed, with similar peak wavelength but a narrower emission profile than the PF, having lost the more red-shifted contributions. Because this narrowed DF corresponds more closely to the higher-energy components of the PF, correlating this with the steady-state spectra, we assign the DF to LE rather than CT emission. At significantly longer times (~2 ms), the red-shifted emission, tentatively assigned as sRTP, becomes dominant.

Crucially, the individual emission spectra extracted at different decay times, shown in Figure S6, illustrate that the ratio of DF to sRTP is not constant over time, which implies that the delayed emission bands cannot arise from two emission mechanisms that scale with triplet concentration in the same way. Based on the very similar spectra of the sRTP and phosphorescence emission at low temperature from zeonex films (Figure S7), we are confident to assign the millisecond emission to sRTP with the small spectral red-shift of sRTP in toluene arising from the ability of the molecules to structurally and energetically relax in fluid solution before emission. Ultimately, this sRTP emission corresponds to a mono-excitonic emission process, while if the DF were to also arise from mono-excitonic TADF (or other upper state crossing mechanisms), the intensity ratio between the DF and sRTP would be expected to remain constant throughout the decay as both processes would draw from the same triplet reservoir. Instead, the stronger LE delayed singlet emission at early times, when the triplet exciton concentration is higher, is fully consistent with a bi-excitonic TTA delayed emission mechanism that populates the higher-energy LE singlet state from the energy of two triplet excitons.[6]

Table 4: Spectroscopic data for the three emitter molecules.

Compound	λ_{abs} (nm)[a]	ε ($M^{-1}cm^{-1}$)[b]	λ_{em} (nm)[c]	$\Phi_{f,atm,sol}$[d]	$\Phi_{f,inert,sol}$[e]	$\Phi_{f,atm,film}$[f]	$\Phi_{f,inert,film}$[g]	Φ_Δ[h]
BTaz-Th-DMAC	325 382	21,200 4,700	466	0.08	0.09	0.29	0.29	0.64
BTaz-Th-PXZ	323 402	12,500 3,000	441 511	0.02	0.03	0.09	0.11	0.59
BTaz-Th-PTZ	325 388	18,500 9,300	455 524	0.01	0.02	0.22	0.22	0.96

[a] Absorption maxima in toluene solution. [b] Molar extinction coefficients at the absorption maxima in toluene solution. [c] Fluorescence emission maxima in toluene solution. [d] Photoluminescence quantum yields in toluene solution under normal atmosphere determined vs quinine (Φ_f = 0.58, λ_{exc} = 347 nm in 0.1 M H_2SO_4). [e] Photoluminescence quantum yields in toluene solution under inert atmosphere determined vs quinine (λ_{exc} = 347 nm). [f] Photoluminescence quantum yield of 1 w/w% zeonex films measured in integrating sphere under air with either 390 nm (**BTaz-Th-DMAC** and **BTaz-Th-PTZ**) or 400 nm (**BTaz-Th-PXZ**) excitation. [g] Photoluminescence quantum yield of 1 w/w% zeonex films measured in integrating sphere under nitrogen flow with either 390 nm (**BTaz-Th-DMAC** and **BTaz-Th-PTZ**) or 400 nm (**BTaz-Th-PXZ**) excitation [h] Singlet oxygen quantum yields in toluene solution determined vs coronene (Φ_Δ = 0.90, λ_{exc} = 325 nm in toluene) by monitoring the absorbance of 1,3-DPBF at 414 nm.

10.1002/chem.202301369

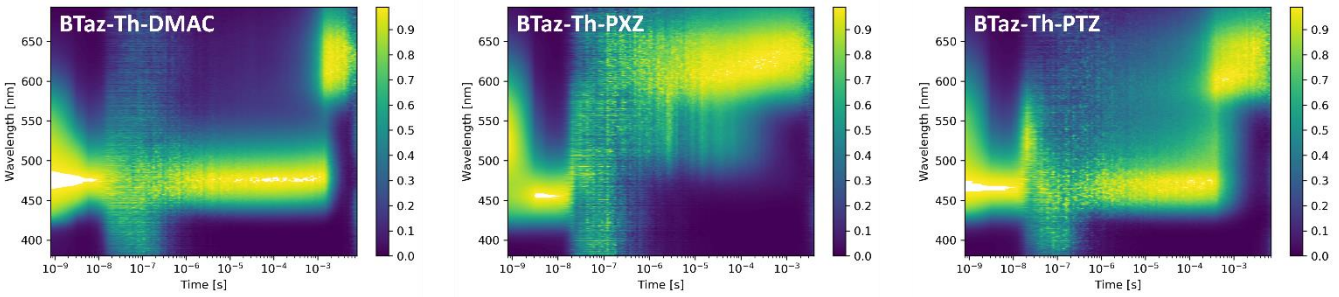

Figure 3: Normalized time-resolved emission spectra for **BTaz-Th-DMAC** (left), **BTaz-Th-PXZ** (middle), and **BTaz-Th-PTZ** (right) in degassed toluene at room temperature.

Similar spectral behavior is observed for **BTaz-Th-PTZ**. The PF from the LE and CT singlet states of **BTaz-Th-PTZ** decays entirely within ~20 ns, followed by blue DF emission from TTA to the LE singlet state from ~1 µs to ~1 ms. Once again, similar to **BTaz-Th-DMAC**, after ~500 µs a red-shifted emission band emerges. This emission is attributed to sRTP based on the spectral similarity to low temperature film measurements, while the varying intensity ratios of blue DF to red sRTP at various times in the crossover regime again allow us to identify the blue DF as arising from TTA. Figure S6 shows that LE emission *via* TTA continues until the ms regime in **BTaz-Th-DMAC** and **BTaz-Th-PTZ** (minor emission peak at higher energy), although the spectra are dominated by sRTP at these low triplet concentrations.

In **BTaz-Th-PXZ**, the PF is also identifiable as arising from a mixture of LE (~450 nm) and CT (~525 nm) contributions, which were readily resolved in the corresponding steady-state emission. The delayed emission in **BTaz-Th-PXZ** can be assigned primarily to sRTP, as previously reported, and we further identify this sRTP as originating from an LE excited state based on the absence of solvatochromic effects when the sRTP was previously recorded in toluene and chloroform solutions.[14] The near-identical sRTP spectra, calculated T_1 energies, and T_1 orbital electron density differences of all three materials here lead us to extend the same excited state character identification to **BTaz-Th-DMAC** and **BTaz-Th-PTZ** as well.

For **BTaz-Th-PXZ**, in the microsecond time region, we note a competing emission band from the same CT singlet state as observed in the PF (Figure S6). Once again the varying ratio of the DF emission bands indicates that the higher energy CT emission may arise from TTA, similar to **BTaz-Th-DMAC** and **BTaz-Th-PTZ** but significantly weaker in this case. Figure 4 also shows that the delayed TTA emission of both **BTaz-Th-DMAC** and **BTaz-Th-PTZ** is more intense than the sRTP of **BTaz-Th-PXZ**, and has a coincidentally similar lifetime (coincidental as sRTP lifetimes are intrinsic material properties, while TTA lifetimes are excitation-power dependent.) Ultimately, we note that the absolute contribution of delayed emission to the total photoluminescence quantum yield – quenched by oxygen when measured in air – is in all cases small, as illustrated in Table 4.

To evaluate the emissive properties of these materials in a solid-state environment, both emission measurements in steady state (Figure S8) and TRES experiments (Figures 5, 6, and S9) were performed in a 1 w/w% zeonex film. As can be seen from the contour plots, the DF attributed to TTA in solution vanishes when the molecules are prevented from diffusing freely and forming bi-excitonic triplet pair states. Instead, the individual spectra shown in Figure S9 reveal strongly red-shifted emission that is attributed to RTP, and which is nearly identical to both the sRTP spectra and to the collected phosphorescence spectra of the same films at 80 K (Figure S10). We also note that the CT contribution to the early PF emission is greatly diminished compared to solution (although still noticeable as shoulders in the steady-state emission, and as a separate later PF contribution in **BTaz-Th-PTZ**). This difference in early CT emission intensity may be due to frustrated electron transfer in the immobilized molecules, causing them to be less able to form stable CT states following excitation. Despite having different initial DF intensities in films, we can conclude from visual inspection of the emission decays that, just as in solution, the RTP emission decays fastest for **BTaz-Th-PXZ**. Similar to the experiments performed in solution, the contribution of the delayed emission to the total emission efficiency is still very small, as illustrated by the air and inert-atmosphere photoluminescence quantum yield measurements in Table 4.

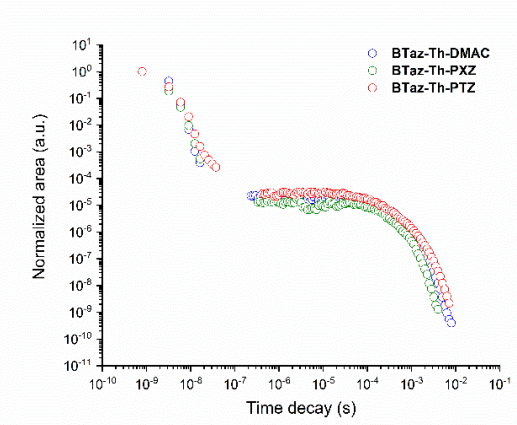

Figure 4: Decay of the total emission (calculated using the integrated area under the emission curve) for for **BTaz-Th-DMAC** (blue), **BTaz-Th-PXZ** (green), and **BTaz-Th-PTZ** (red) in degassed toluene at room temperature. Data points for which the emission signal falls below the hardware noise baseline have been omitted from the decay.

10.1002/chem.202301369

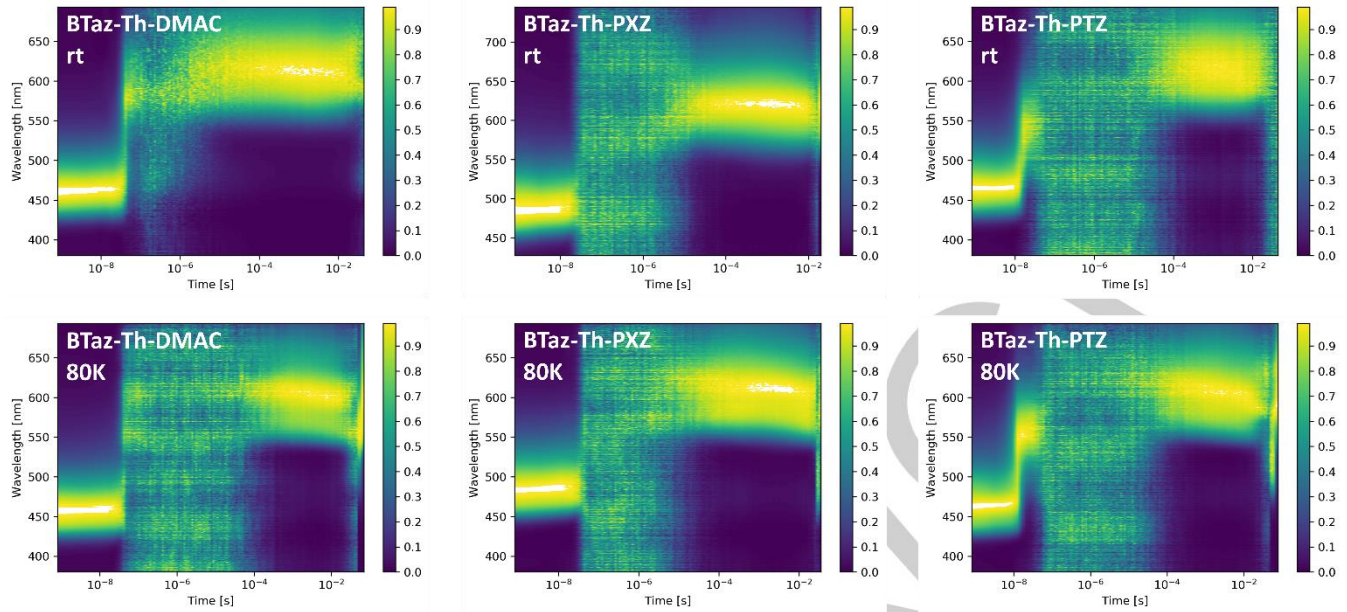

Figure 5: Normalized time-resolved emission spectra for **BTaz-Th-DMAC** (left), **BTaz-Th-PXZ** (middle), and **BTaz-Th-PTZ** (right) in 1 w/w% zeonex films at room temperature (top row) and at 80 K (bottom row).

Typically central to the discussion of TADF materials, the singlet-triplet energy splitting ($\Delta E_{S_1-T_1}$) is obtained experimentally by comparing the onset of the steady-state fluorescence with the onset of the phosphorescence, measured here either at longer time delays at room temperature for toluene, *i.e.* sRTP, or at 80 K for zeonex films, *i.e.* typical phosphorescence (Figure S7 and S10, respectively). $\Delta E_{S_1-T_1}$ values were determined for the three dyads and are shown in Table 5. In contrast to our previous work,[14] where changing the π-bridge resulted in a change in T_1 while S_1 remained the same for all three compounds, here a change in S_1 is observed upon altering the donor unit, whereas T_1 remains approximately the same for all materials. However, due to the strongly overlapping CT and LE bands (Figure 2, S6), we have to take the estimated CT onset from steady-state spectra.

The relative energies of the excited states can be used to understand the emission mechanisms. A schematic representation of the excited state energy levels of interest with their corresponding CT or LE character, as obtained using TDDFT calculations and experimentally in toluene, is shown in Figure 7. For **BTaz-Th-PXZ**, both theory and experiment point to a clear decrease of both S_1 and T_2 with respect to **BTaz-Th-DMAC** and **BTaz-Th-PTZ**. Furthermore, both the theoretical and experimental data show that for all three compounds, T_1 remains almost identical. This indicates that T_1 has LE character and originates predominately from the BTaz-Th acceptor part (as confirmed by calculations; see Table S1 and Figures S11-S12), and we again suggest that the differences in RTP onset energy observed in toluene and zeonex (~200 meV lower in toluene) arise from geometric relaxation that is possible in fluid toluene but not in the rigid polymer. Solvatochromic changes in RTP energy were not previously observed for **BTaz-Th-PXZ** in toluene and chloroform, which excludes the sRTP having CT character.[14] This is further confirmed by Figures 7 and S13, where the calculated and experimentally determined excited states are depicted for this accepting unit (**BTaz-Th**, which was additionally synthesized, measured and calculated as a reference compound; see Scheme 2, Figures S11-14 and Tables S1-S4).

We first identify that the experimental $\Delta E_{S_1-T_1}$ is smallest for sRTP-active **BTaz-Th-PXZ**, but is still large compared to the TADF-active materials[14] (and accordingly, we do not observe TADF emission for any of the present materials). Additionally, the theoretically determined $\Delta E_{T_2-T_1}$ is also significantly smaller for **BTaz-Th-PXZ** compared to **BTaz-Th-DMAC** and **BTaz-Th-PTZ**. We note that the observed ^{3}LE emission is formally spin-forbidden, and so explanations for the faster sRTP in **BTaz-Th-PXZ** must ultimately address this restriction. To make sRTP more plausible under these circumstances, there are two different processes that could increase the ^{3}LE emission discussed below.

A first process that could allow sRTP to occur is a coupling of the ^{3}LE (T_1) state with the ^{1}CT (S_1) due to the smaller $\Delta E_{S_1-T_1}$ of **BTaz-Th-PXZ** relative to **BTaz-Th-DMAC** and **BTaz-Th-PTZ**. Consequently, this coupling distorts the exclusive triplet character of the T_1 state, receiving singlet character and resulting in a more allowed transition to the ground state, hence facilitating the phosphorescent decay.[19]

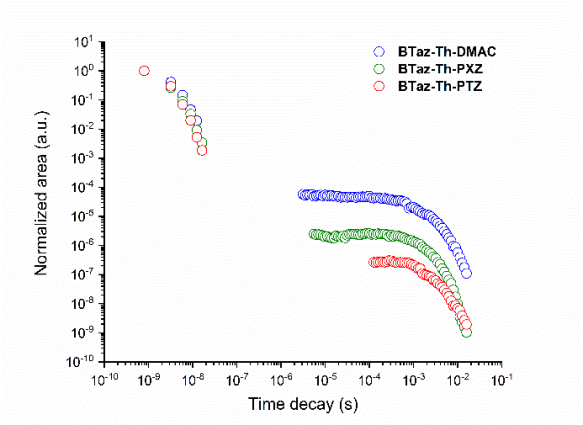

Figure 6: Decay of the total emission (calculated using the integrated area under the emission curve) for for **BTaz-Th-DMAC** (blue), **BTaz-Th-PXZ** (green), and **BTaz-Th-PTZ** (red) in zeonex at room temperature. Data points for which the emission signal falls below the hardware noise baseline have been omitted from the decay.

Table 5: Singlet and triplet energies derived both theoretically and experimentally (from the steady-state and time-resolved emission spectra, respectively, in a 50 µM toluene solution and a 1 w/w% zeonex film).

	Toluene					Zeonex				
Compound	E_{S_1} (eV)[a]	E_{T_1} (eV)[c]	E_{T_2} (eV)[c]	$\Delta E_{S_1-T_1}$ (eV)[d]	$\Delta E_{T_2-T_1}$ (eV)[e]	E_{S_1} (eV)[a]	E_{T_1} (eV)[c]	E_{T_2} (eV)[c]	$\Delta E_{S_1-T_1}$ (eV)[d]	$\Delta E_{T_2-T_1}$ (eV)[e]
BTaz-Th-DMAC	3.12	2.77	3.11	0.35	0.34	-	-	3.11	-	0.69
	(2.97)	(2.25)	-	(0.72)	(0.86)	(3.01)	(2.42)	-	(0.59)	
BTaz-Th-PXZ	2.86	2.78	2.85	0.08	0.07	-	-	2.85	-	0.45
	(2.81)	(2.25)	-	(0.56)	(0.60)	(2.84)	(2.40)	-	(0.44)	
BTaz-Th-PTZ	3.19	2.76	3.14	0.43	0.38	-	-	3.14	-	0.71
	(3[b])	(2.25)	-	(0.75)	(0.89)	(3[d])	(2.43)	-	(0.57)	

[a] From TDDFT (or best estimate from experiments in brackets). [b] CT singlet onset, estimated from steady-state spectra, limited by strong overlap with LE emission. [c] From TDDFT or in brackets taken from the onset of the sRTP emission at ms timescales, or from film phosphorescence at 80 K in zeonex. [d] Calculated as $E_{S_1} - E_{T_1}$ from either calculated (or experimental) values. [e] Calculated as $E_{T_2} - E_{T_1}$ from calculated and experimental values, respectively.

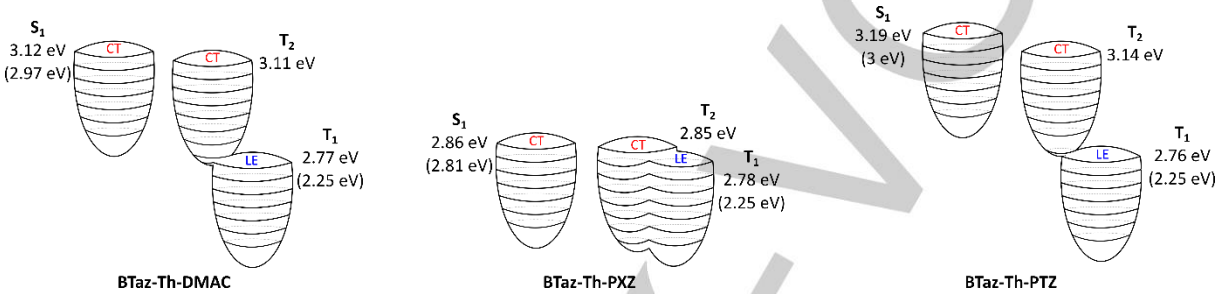

Figure 7: Schematic representation of the excited state energy levels with their corresponding CT/LE character as obtained using TDDFT calculations with LC-BLYP (ω = 0.17 bohr^{-1})/6-311G(d) under the TDA and applying the PCM (cyclohexane). The values obtained experimentally in toluene are added between brackets.

A second possible process is a coupling between the ^{3}LE (T_1) and the ^{3}CT (T_2) states. This coupling will be strongest in **BTaz-Th-PXZ** due to the relatively smaller $\Delta E_{T_1-T_2}$, although all three materials have significant SOC for the $T_2 \rightarrow S_0$ transition (Table 3). This large SOC enables a flip of the spin multiplicity, accelerating a radiative transition between a triplet state and the ground state, *i.e.* phosphorescence, and most effectively so for **BTaz-Th-PXZ**.

Due to the small energy differences between the CT S_1 and T_2 states in these materials, both the $\Delta E_{S_1-T_1}$ and $\Delta E_{T_2-T_1}$ values follow the same trend and can be used interchangeably. Consequently, both potential coupling mechanisms that accelerate phosphorescence and allow sRTP in **BTaz-Th-PXZ** are possible, and may even be working in tandem rather than exclusively. Although we are not able to distinguish between them experimentally, we can firmly conclude that RTP and sRTP in these materials are not exclusively related to the coupling between the T_1 state and the ground state. Instead, energy gaps and coupling to excited states with higher energy (either S_1, T_2, or a combination of both) significantly control the emission mechanism.

In contrast, for **BTaz-Th-DMAC** and **BTaz-Th-PTZ**, the calculated and experimental energy gaps between both S_1 and T_1, and T_1 and T_2, are significantly larger, lowering the coupling efficiency between the ^{3}LE and an excited CT state higher in energy. This relegates triplet emission to a slower rate and allows TTA to outcompete it in solution. The intrinsic emissivity of the LE T_1 allows long-lived RTP to arise once triplet exciton concentrations have fallen to low enough levels for TTA to become inactive. Nonetheless, this residual sRTP, observed at the latest delay times for **BTaz-Th-DMAC** and **BTaz-Th-PTZ,** still decays more slowly than the dominant sRTP in **BTaz-Th-PXZ** (Figure 4). In further contrast to the presented materials, if these energy gaps are reduced too much (< ~0.4 eV), it instead allows TADF processes to outcompete phosphorescence,[14] and so a delicate balance of energy gaps is required to promote elusive sRTP emission properties. Separate from the emissive properties, relatively slow TTA and sRTP in **BTaz-Th-PTZ** combined with significant sulfur-assisted ISC also allows ample time for oxygen to quench excited triplets, leading to its impressively large singlet oxygen quantum yield.

Conclusions

In this work, we investigate the material properties that support sRTP emission pathways. In contrast to previous work in which the π-bridge was altered, here the T_1 state remains the same for all three compounds, while both the S_1 and T_2 states shift significantly as we change the donor. Consequently, this leads to a complex interplay between the excited states, causing different emission mechanisms, including TTA and exceedingly rare sRTP. From experiments and TDDFT calculations we find that the energy gaps between the emissive T_1 state and CT-character S_1 and T_2 states are relatively lower for **BTaz-Th-PXZ**, with resulting smaller $\Delta E_{S_1-T_1}$ and $\Delta E_{T_2-T_1}$, allowing coupling with the LE-character T_1 state. This coupling and transfer of singlet character and/or $T_2 \rightarrow S_0$ SOC results in accelerated ^{3}LE decay and almost exclusive RTP emission, with only a small contribution of TTA from the CT singlet, even in solution. The larger energy differences for **BTaz-Th-DMAC** and **BTaz-Th-PTZ** prevent similar excited state coupling from accelerating RTP emission channels in these materials, resulting instead in dominant TTA emission in solution. When these energy gaps are reduced further, exclusively TADF is observed. We therefore uncover an optimum

energy splitting between T_1 and S_1 and/or T_2 that is large enough to prevent TADF, but still small enough to enhance sRTP and allow it to outcompete solution TTA. Recognizing the importance of coupling to higher excited states will help direct future understanding and eventual applications of this rare and elusive sRTP phenomenon.

Experimental Section

2-(5-bromothiophen-2-yl)benzo[*d*]thiazole (**BTaz-Th-Br**)[14]
General procedure 1: 5-Bromothiophene-2-carbaldehyde (280 µL, 2.35 mmol), 2-aminobenzenethiol (289.2 mg, 2.31 mmol), and sodium metabisulfite (448 mg, 2.36 mmol) were dissolved in DMF (10 mL), and the mixture was stirred under reflux for 2 h. Afterward, the reaction mixture was cooled down to room temperature, water was added, and an extraction with ethyl acetate was performed. The combined organic phase was dried over anhydrous $MgSO_4$, filtered, and concentrated under reduced pressure. The crude product was purified by column chromatography (silica) with CH_2Cl_2/petroleum ether (v/v = 40/60) as the eluent. 2-(5-Bromothiophen-2-yl)benzo[*d*]thiazole was obtained as a yellow solid in 17% yield (118.3 mg). ^{1}H NMR (400 MHz, $CDCl_3$): δ = 8.00 (d, *J* = 8.1 Hz, 1H), 7.82 (d, *J* = 8.1 Hz, 1H), 7.49–7.44 (m, 1H), 7.39–7.33 (m, 1H), 7.06 (d, *J* = 4.0 Hz, 1H). ^{13}C NMR (100 MHz, $CDCl_3$): δ = 160.4, 153.6, 138.9, 134.6, 131.1, 128.6, 126.7, 125.6, 123.2, 121.7, 117.3. MS (ESI+) Calcd. for $C_{11}H_6BrNS_2$ $[M+H]^+$: *m/z* 295.9203 (100%), found: 295.9186.

10-(5-(benzo[*d*]thiazol-2-yl)thiophen-2-yl)-10H-phenoxazine (**BTaz-Th-PXZ**)[14]
General procedure 2 (Buchwald-Hartwig coupling): 2-(5-Bromothiophen-2-yl)benzo[*d*]thiazole (118 mg, 398 µmol), 10H-phenoxazine (79.2 mg, 432 µmol), palladium(II) acetate (8.9 mg, 40 µmol), tri-*tert*-butylphosphine (16.1 mg, 80 µmol), and sodium *tert*-butoxide (76.6 mg, 797 µmol) were dissolved in dry toluene (12 mL) under argon atmosphere. The mixture was heated to reflux for 16 h while stirring and then cooled down to room temperature and concentrated under reduced pressure. The crude product was purified by column chromatography (silica) with CH_2Cl_2/petroleum ether (v/v = 40/60) as the eluent. **BTaz-Th-PXZ** was further purified using preparative (recycling) size exclusion chromatography and was obtained as a yellow solid (115.8 mg, 75%). ^{1}H NMR (400 MHz, $CDCl_3$): δ = 8.04 (d, *J* = 8.1 Hz, 1H), 7.89 (d, *J* = 8.0 Hz, 1H), 7.70 (d, *J* = 3.9 Hz, 1H), 7.53–7.47 (m, 1H), 7.43–7.38 (m, 1H), 7.07 (d, *J* = 3.9 Hz, 1H), 6.78–6.70 (m, 6H), 6.40 (dt, *J* = 7.3, 1.2 Hz, 2H). ^{13}C NMR (100 MHz, $CDCl_3$): δ = 161.0, 153.7, 144.1, 137.5, 134.8, 133.6, 129.7, 127.9, 126.8, 125.7, 123.7, 123.4, 122.8, 121.7, 115.9, 114.4. MS (ESI+) Calcd. for $C_{23}H_{15}N_2OS_2$ $[M+H]^+$: *m/z* 399.0626 (100%), found: 399.0606.

2-(5-(9,9-dimethylacridin-10(9*H*)-yl)thiophen-2-yl)benzo[*d*]thiazole (**BTaz-Th-DMAC**)
Synthesis according to general procedure 2: 2-(5-Bromothiophen-2-yl)benzo[*d*]thiazole (220 mg, 743 µmol), 9,9-dimethyl-9,10-dihydroacridine (171 mg, 817 µmol), palladium(II) acetate (16.7 mg, 74 µmol), tri-*tert*-butylphosphine (30.1 mg, 149 µmol), sodium *tert*-butoxide (142.8 mg, 1.49 mmol), dry toluene (12 mL), eluent CH_2Cl_2/petroleum ether (v/v = 40/60); yellow solid (19.2 mg, 6%). ^{1}H NMR (400 MHz, $CDCl_3$): δ = 8.04 (d, *J* = 8.1 Hz, 1H), 7.89 (d, *J* = 8.1 Hz, 1H), 7.76 (d, *J* = 3.9 Hz, 1H), 7.53–7.45 (m, 3H), 7.44–7.38 (m, 1H), 7.16–7.10 (m, 2H), 7.08 (d, *J* = 3.7 Hz, 1H), 7.07–7.02 (m, 2H), 6.88–6.84 (m, 2H), 1.70 (s, 6H). ^{13}C NMR (100 MHz, $CDCl_3$): δ = 161.3, 153.8, 147.3, 140.8, 136.6, 134.8, 131.6, 128.7, 128.0, 126.8, 126.7, 125.6, 125.3, 123.3, 122.2, 121.7, 115.2, 36.1, 31.2. MS (ESI+) Calcd. for $C_{26}H_{20}N_2S_2$ $[M+H]^+$: *m/z* 425.1073 (100%), found: 425.1066.

10-(5-(benzo[*d*]thiazol-2-yl)thiophen-2-yl)-10*H*-phenothiazine (**BTaz-Th-PTZ**)
Synthesis according to general procedure 2: 2-(5-Bromothiophen-2-yl)benzo[*d*]thiazole (107 mg, 675 µmol), 10*H*-phenothiazine (148 mg, 742 µmol), palladium(II) acetate (15.1 mg, 68 µmol), tri-*tert*-butylphosphine (27.3 mg, 135 µmol), sodium *tert*-butoxide (129.8 mg, 1.35 mmol), dry toluene (12 mL), eluent CH_2Cl_2/petroleum ether (v/v = 40/60); yellow solid (110 mg, 38%). ^{1}H NMR (400 MHz, $CDCl_3$): δ = 7.99 (d, *J* = 7.7 Hz, 1H), 7.85 (d, *J* = 7.9 Hz, 1H), 7.57 (d, *J* = 4.0 Hz, 1H), 7.51–7.42 (m, 1H), 7.40–7.32 (m, 1H), 7.19 (dd, *J* = 7.6, 1.3 Hz, 2H), 7.15–7.05 (m, 4H), 7.05–6.99 (m, 2H), 6.88 (d, *J* = 4.0 Hz, 1H). ^{13}C NMR (100 MHz, $CDCl_3$): δ = 161.7, 154.1, 151.0, 143.6, 135.0, 132.4, 128.6, 127.9, 127.9, 127.6, 127.0, 125.9, 125.7, 125.2, 123.4, 122.6, 122.0, 120.3. MS (ESI+) Calcd. for $C_{23}H_{14}N_2S_3$ $[M+H]^+$: *m/z* 415.0325 (100%), found 415.0334.

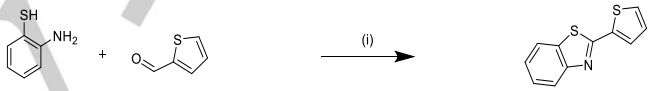

Scheme 2. Synthesis procedure for the reference compound **BTaz-Th**: (i) sodium metabisulfite, DMF, reflux, 2 h.

2-(thiophen-2-yl)benzo[*d*]thiazole (**BTaz-Th**)
Synthesis according to general procedure 1: Thiophene-2-carbaldehyde (1.000 g, 8.92 mmol), 2-aminobenzenethiol (1.228 g, 9.808 mmol), sodium metabisulfite (1.865 g, 9.808 mmol), DMF (25 mL), eluent CH_2Cl_2/petroleum ether (v/v = 40/60); (2.035 g, 77%). ^{1}H NMR (400 MHz, $CDCl_3$): δ = 8.08 (d, *J* = 8.1 Hz, 1H), 7.88–7.85 (m, 1H), 7.79 (dd, *J* = 3.7, 1.2 Hz, 1H), 7.54 (dd, *J* = 5.0, 1.2 Hz, 1H), 7.52–7.48 (m, 1H), 7.42–7.37 (m, 1H), 7.18–7.15 (m, 1H). ^{13}C NMR (100 MHz, $CDCl_3$) δ = 161.9, 152.7, 136.6, 134.2, 130.1, 129.6, 128.5, 126.9, 125.7, 122.8, 121.7. MS (ESI+) Calcd. for $C_{11}H_7NS_2$ 11 $[M+H]^+$: *m/z* 218.00 (100%), found: 218.01.

Acknowledgements

The authors thank the Research Foundation – Flanders (FWO Vlaanderen) for financial support (projects G087718N, G0D1521N, I006320N, GOH3816NAUHL, the Scientific Research Community 'Supramolecular Chemistry and Materials' (W000620N), and Ph.D. scholarship S. Paredis). The calculations were performed on the computers of the 'Consortium des équipements de Calcul Intensif (CÉCI)' (http://www.ceci-hpc.be), including those of the 'UNamur Technological Platform of High-Performance Computing (PTCI)' (http://www.ptci.unamur.be), for which we gratefully acknowledge financial support from the FNRS-FRFC, the Walloon Region, and the University of Namur (Conventions No. GEQ U.G006.15, U.G018.19, U.G011.22, RW/GEQ2016, RW1610468, and RW2110213). A.P. Monkman is supported by EPSRC grant EP/T02240X/1.

Keywords: donor-acceptor fluorophores • room temperature phosphorescence • energy gap tuning • time-resolved spectroscopy

[1] a) J. Zhi, Q. Zhou, H. Shi, Z. An and W. Huang, *Chem. Asian. J.*, **2020**, 15, 947–957; b) C. Sun, X. Ran, X. Wang, Z. Cheng, Q. Wu, S. Cai, L. Gu, N. Gan, H. Shi, Z. An, H. Shi and W. Huang, *J. Phys. Chem. Lett.*, **2018**, 9, 335–339; c) G. Yang, A. Lv, Z. Xu, Z. Song, K. Shen, C. Lin, G. Niu, H. Ma, H. Shi and Z. An, *J. Mater. Chem. C*, **2022**, 10, 13747–13752.

[2] a) X. Zhang, Y. Hou, X. Xiao, X. Chen, M. Hu, X. Geng, Z. Wang and J. Zhao, *Coord. Chem. Rev.*, **2020**, 417, 213371; b) H. Xu, R. Chen, Q. Sun, W. Lai, Q. Su, W. Huang and X. Liu, *Chem. Soc. Rev.*, **2014**, 43, 3259–3302.

[3] W.-Y. Wong and C.-L. Ho, *J. Mater. Chem.*, **2009**, 19, 4457–4482.

[4] a) Y. Song, J. Wang, L. Chen and P. Yang, *J. Lumin.*, **2020**, 225, 117325; b) S. Kuno, T. Kanamori, Z. Yijing, H. Ohtani and H. Yuasa, *ChemPhotoChem*, **2017**, 1, 102–106; c) H. F. Higginbotham, M. Okazaki, P. de Silva, S. Minakata, Y. Takeda and P. Data, *ACS. Appl. Mater. Interfaces*, **2021**, 13, 2899–2907.

[5] a) Y. Ning, J. Yang, H. Si, H. Wu, X. Zheng, A. Qin and B. Z. Tang, *Sci. China. Chem.*, **2021**, 64, 739–744; b) Meng, S. Guo, B. Jiang, X. Zhang, L. Zou, C. Wei, Y. Gong, S. Wu and Y. Liu, *J. Mater. Chem. C*, **2021**, 9, 8515–8523; c) G. Farias, C. A. M. Salla, M. Aydemir, L. Sturm, P. Dechambenoit, F. Durola, B. de Souza, H. Bock, A. P. Monkman and I. H. Bechtold, *Chem. Sci.*, **2021**, 12, 15116–15127; d) A. M. Salla, G. Farias, M. Rouzières, P. Dechambenoit, F. Durola, H. Bock, B. de Souza and I. H. Bechtold, *Angew. Chem. Int. Ed.*, **2019**, 58, 6982–6986; *Angew. Chem.*, **2019**, 131, 7056–7060.

[6] A. Danos, R. W. MacQueen, Y. Y. Cheng, M. Dvořák, T. A. Darwish, D. R. McCamey and T. W. Schmidt, *J. Phys. Chem. Lett.*, **2015**, 6, 3061–3066.

[7] Y. Y. Cheng, B. Fückel, T. Khoury, R. G. C. R. Clady, M. J. Y. Tayebjee, N. J. Ekins-Daukes, M. J. Crossley and T. W. Schmidt, *J. Phys. Chem. Lett.*, **2010**, 1, 1795–1799.

[8] a) Y. Liu, C. Li, Z. Ren, S. Yan and M. R. Bryce, *Nat. Rev. Mater.*, **2018**, 3, 18020; b) M. Cai, D. Zhang and L. Duan, *Chem. Rec.*, **2019**, 19, 1611–1623; c) H. Nakanotani, Y. Tsuchiya and C. Adachi, *Chem. Lett.*, **2021**, 50, 938–948; d) D. Volz, *J. Photon. Energy*, **2016**, 6, 020901; e) F. B. Dias, T. J. Penfold and A. P. Monkman, *Methods Appl. Fluoresc.*, **2017**, 5, 012001; f) M. Y. Wong and E. Zysman-Colman, *Adv. Mater.*, **2017**, 29, 1605444.

[9] A. P. Monkman, C. Rothe and S. M. King, *Proc. IEEE*, **2009**, 97, 1597–1605.

[10] a) Y. Li, L. Jiang, W. Liu, S. Xu, T. Li, F. Fries, O. Zeika, Y. Zou, C. Ramanan, S. Lenk, R. Scholz, D. Andrienko, X. Feng, K. Leo and S. Reineke, *Adv. Mater.*, **2021**, 33, 2101844; b) W. Zhao, Z. He and B. Z. Tang, *Nat. Rev. Mater.*, **2020**, 5, 869–885.

[11] I. A. Wright, A. Danos, S. Montanaro, A. S. Batsanov, A. P. Monkman and M. R. Bryce, *Chem. Eur. J.*, **2021**, 27, 6545–6556.

[12] A. Maggiore, X. Tan, A. Brosseau, A. Danos, F. Miomandre, A. P. Monkman, P. Audebert and G. Clavier, *Phys. Chem. Chem. Phys.*, **2022**, 24, 17770–17781.

[13] C. Xu, X. Lin, W. Wu and X. Ma, *Chem. Commun.* **2021**, 57, 10178–10181.

[14] S. Paredis, T. Cardeynaels, J. Deckers, A. Danos, D. Vanderzande, A. P. Monkman, B. Champagne and W. Maes, *J. Mater. Chem. C*, **2022**, 10, 4775–4784.

[15] a) Z.-Y. Zhang, Y. Chen and Y. Liu, *Angew. Chem. Int. Ed.*, **2019**, 58, 6028–6032; *Angew. Chem.*, **2019**, 131, 6089–6093; b) J. Wang, Z. Huang, X. Ma and H. Tian, *Angew. Chem. Int. Ed.*, **2020**, 59, 9928–9933; *Angew. Chem.*, **2020**, 132, 10014–10019; c) H. Chen, X. Ma, S. Wu and H. Tian, *Angew. Chem. Int. Ed.*, **2014**, 53, 14149–14152; *Angew. Chem.*, **2014**, 126, 14373–14376; d) W.-L. Zhou, Y. Chen, Q. Yu, H. Zhang, Z.-X. Liu, X.-Y. Dai, J.-J. Li and Y. Liu, *Nat. Commun.*, **2020**, 11, 4655; e) F.-F. Shen, Y. Chen, X. Dai, H.-Y. Zhang, B. Zhang, Y. Liu and Y. Liu, *Chem. Sci.*, **2021**, 12, 1851–1857; f) H.-J. Yu, Q. Zhou, X. Dai, F.-F. Shen, Y.-M. Zhang, X. Xu and Y. Liu, *J. Am. Chem. Soc.*, **2021**, 143, 13887−13894.

[16] a) S. Kuila, K. V. Rao, S. Garain, P. K. Samanta, S. Das, S. K. Pati, M. Eswaramoorthy and S. J. George, *Angew. Chem. Int. Ed.*, **2018**, 57, 17115–17119; *Angew. Chem.*, **2018**, 130, 17361–17365; b) S. Garain, B. C. Garain, M. Eswaramoorthy, S. K. Pati and S. J. George, *Angew. Chem. Int. Ed.*, **2021**, 60, 19720–19724; *Angew. Chem.*, **2021**, 133, 19872–19876.

[17] a) J. Xu, A. Takai, Y. Kobayashi and M. Takeuchi, *Chem. Commun.*, **2013**, 49, 8447–8449; b) G. D. Gutierrez, G. T. Sazama, T. Wu, M. A. Baldo and T. M. Swager, *J. Org. Chem.*, **2016**, 81, 4789–4796; c) H. M. Luciano, G. Farias, C. M. Salla, L. G. Franca, S. Kuila, A. P. Monkman, F. Durola, I. H. Bechtold, H. Bock and H. Gallardo, *Chem. Eur. J.*, **2023**, e202203800.

[18] a) X. Zhen, Y. Tao, A. An, P. Chen, C. Xu, R. Chen, W. Huang and K. Pu, *Adv. Mater.*, **2017**, 29, 1606665; b) Y. Wang, H. Gao, J. Yang, M. Fang, D. Ding, B. Z. Tang and Z. Li, *Adv. Mater.*, **2021**, 33, 2007811.

[19] a) L. F. Cooley, H. Han and M. B. Zimmt, *J. Phys. Chem. A*, **2002**, 106, 884–892; b) M. Kojić, I. Lyskov, B. Milovanović, C. M. Marian and M. Etinski, *Photochem. Photobiol. Sci.*, **2019**, 18, 1324–1332; c) G. Baryshnikov, B. Minaev and H. Ågren, *Chem. Rev.*, **2017**, 117, 6500–6537.

[20] X. Liu, A. Li, W. Xu, Z. Ma and X. Jia, *Mater. Chem. Front.*, **2019**, 3, 620–625.

[21] T. Cardeynaels, S. Paredis, J. Deckers, S. Brebels, D. Vanderzande, W. Maes and B. Champagne, *Phys. Chem. Chem. Phys.*, **2020**, 22, 16387–16399.

[22] M. J. Frisch, G. W. Trucks, H. B. Schlegel, G. E. Scuseria, M. A. Robb, J. R. Cheeseman, G. Scalmani, V. Barone, G. A. Petersson, H. Nakatsuji, X. Li, M. Caricato, A. V. Marenich, J. Bloino, B. G. Janesko, R. Gomperts, B. Mennucci, H. P. Hratchian, J. V. Ortiz, A. F. Izmaylov, J. L. Sonnenberg, D. Williams-Young, F. Ding, F. Lipparini, F. Egidi, J. Goings, B. Peng, A. Petrone, T. Henderson, D. Ranasinghe, V. G. Zakrzewski, J. Gao, N. Rega, G. Zheng, W. Liang, M. Hada, M. Ehara, K. Toyota, R. Fukuda, J. Hasegawa, M. Ishida, T. Nakajima, Y. Honda, O. Kitao, H. Nakai, T. Vreven, K. Throssell, J. A. Montgomery Jr., J. E. Peralta, F. Ogliaro, M. J. Bearpark, J. J. Heyd, E. N. Brothers, K. N. Kudin, V. N. Staroverov, T. A. Keith, R. Kobayashi, J. Normand, K. Raghavachari, A. P. Rendell, J. C. Burant, S. S. Iyengar, J. Tomasi, M. Cossi, J. M. Millam, M. Klene, C. Adamo, R. Cammi, J. W. Ochterski, R. L. Martin, K. Morokuma, O. Farkas, J. B. Foresman and D. J. Fox, Gaussian 16, revision A.03, Gaussian, Inc., Wallingford CT, **2016**.

[23] T. Le Bahers, C. Adamo and I. Ciofini, *J. Chem. Theory Comput.*, **2011**, 7, 2498–2506.

[24] X. Gao, S. Bai, D. Fazzi, T. Niehaus, M. Barbatti and W. Thiel, *J. Chem. Theory Comput.*, **2017**, 13, 515–524.

[25] a) J. Luo, C. Yang, B. Tong, J. Zheng, J. Ma, L. Liang and M. Lu, *J. Photochem. Photobiol. A Chem.*, **2011**, 222, 241–248; b) Z. Shen, R. Procházka, J. Daub, N. Fritz, N. Acar and S. Schneider, *Phys. Chem. Chem. Phys.*, **2003**, 5, 3257–3269.

[26] M. K. Etherington, F. Franchello, J. Gibson, T. Northey, J. Santos, J. S. Ward, H. F. Higginbotham, P. Data, A. Kurowska, P. L. dos Santos, D. R. Graves, A. S. Batsanov, F. B. Dias, M. R. Bryce, T. J. Penfold and A. P. Monkman, *Nat. Commun.*, **2017**, 8, 14987.

10.1002/chem.202301369

WILEY-VCH

RESEARCH ARTICLE

Entry for the Table of Contents

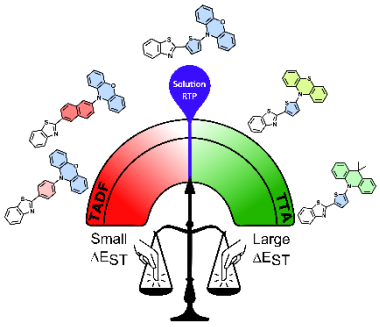

Solution-phase room temperature phosphorescence is very rare in all-organic emitters. Here we show how this property can emerge as a function of energy gaps between the phosphorescent state and higher energy charge-transfer states. An optimal gap of ~0.4 eV yields efficient phosphorescence, with smaller gaps leading to thermally activated delayed fluorescence and larger gaps allowing triplet-triplet annihilation to dominate.

Institute and/or researcher Twitter usernames: Wouter Maes - DSOS research group (@woutermaes_dsos)